# Phase transition of strongly interacting matter with a chemical potential dependent Polyakov loop potential

Guo-yun Shao,[1,*] Zhan-duo Tang,[1] Massimo Di Toro,[2,3] Maria Colonna,[2] Xue-yan Gao,[1] and Ning Gao[1]

[1]*Department of Applied Physics, Xi'an Jiaotong University, Xi'an 710049, China*
[2]*INFN-Laboratori Nazionali del Sud, Via S. Sofia 62, Catania I-95123, Italy*
[3]*Physics and Astronomy Department, University of Catania, Via S. Sofia 64, Catania I-95123, Italy*

We construct a hadron-quark two-phase model based on the Walecka-quantum hadrodynamics and the improved Polyakov–Nambu–Jona-Lasinio (PNJL) model with an explicit chemical potential dependence of Polyakov loop potential ($\mu$PNJL model). With respect to the original PNJL model, the confined-deconfined phase transition is largely affected at low temperature and large chemical potential. Using the two-phase model, we investigate the equilibrium transition between hadronic and quark matter at finite chemical potentials and temperatures. The numerical results show that the transition boundaries from nuclear to quark matter move towards smaller chemical potential (lower density) when the $\mu$-dependent Polyakov loop potential is taken. In particular, for charge asymmetric matter, we compute the local asymmetry of $u$, $d$ quarks in the hadron-quark coexisting phase, and analyze the isospin-relevant observables possibly measurable in heavy-ion collision (HIC) experiments. In general new HIC data on the location and properties of the mixed phase would bring relevant information on the expected chemical potential dependence of the Polyakov loop contribution.

## I. INTRODUCTION

The exploration of the QCD phase diagram of strongly interacting matter and the transition signatures from nuclear to quark-gluon matter are subjects of great interest in recent decades. Intensive searches on high-energy heavy-ion collision (HIC) have been performed in laboratories such as RHIC and LHC, and a near perfect fluid of quark-gluon plasma (QGP) has been created [1]. Further experiments to look for the critical end point (CEP) and the boundaries of the phase transition are in the plan in the next generation facilities such as the second stage of the beam energy scan (BES II) project on RHIC and programs on NICA/FAIR/J-PARC. In particular, experiments will be performed in the region of high baryon density where a promising observation of the signatures of the phase transformation is being looked forward to.

Ultimately these phenomena have to be understood in the frame of quantum chromodynamics (QCD). However, in spite of tremendous theoretical and experimental efforts, the QCD phase diagram has not been unveiled yet [2,3]. In particular, at finite chemical potential $\mu_B$, the situation is not clear. Lattice QCD simulation is a fundamental tool to investigate the thermodynamics of QCD matter at vanishing and/or small chemical potential [4–9], but it suffers the sign problem of the fermion determinant with three colors at finite baryon chemical potential. Some approximation

methods have been proposed to try to overcome the problem, however, the region of large chemical potential and low temperature essentially remains inaccessible [10–13].

In addition to the lattice QCD simulation, kinds of quantum field theory approaches and phenomenological models, such as the Dyson-Schwinger equation approach [14–19], the Nambu–Jona-Lasinio (NJL) model [20–31], the PNJL model [32–38], the entanglement extended PNJL model [39–45], and the Polyakov loop extended quark-meson (PQM) model [46–48], have been developed to give a complete description of QCD matter.

Among these models, the PNJL model which takes into account both the chiral dynamics and (de)confinement effect at high temperature, gives a good reproduction of lattice data at vanishing chemical potential. On the other hand, in the original PNJL model, a "quarkyonic phase" in which the quarks are confined but the dynamical chiral symmetry is already restored appear at high density and finite $T$ [49,50]. In theory, quark deconfinement should also occur at high density. The absence of quark deconfinement at low $T$ and high density in the original PNJL model originates from that the Polyakov loop potential is extracted from pure Yang-Mills lattice simulation at vanishing $\mu_B$. In the presence of dynamical quarks, the contribution from the matter sector and its quantum backreaction to the glue sector should be included. This can realized by introducing a flavor and chemical potential dependent Polyakov loop potential in the functional

---
*Corresponding author.
gyshao@mail.xjtu.edu.cn

renormalization group (FRG) approach [51]. With the incorporation of both the matter and glue dynamics, the flavor and chemical potential dependent Polyakov loop potential has been taken in the PQM model [51–53] and the PNJL model [54,55] to study the full QCD phase diagram and thermodynamics. The calculations show that the chiral restoration and deconfinement transition almost coincide at low $T$ and large $\mu_B$ region [52,55].

All these effective models describe strongly interacting matter based on quark degrees of freedom. Baryons are not treated in these models. However, as far as we know, the strongly interacting matter is governed by hadronic degrees of freedom at low $T$ and small $\mu_B$. When we investigate the phase transformation from nuclear to quark matter, it is practical to describe nuclear matter based on the hadronic degrees of freedom at low $T$ and small $\mu_B$, but quark matter with quark-gluon degrees of freedom at high $T$ and large $\mu_B$. The phase transition boundaries can be derived by constructing an equilibrium phase transition between hadronic and quark matter, possibly reached in the interior of compact stars and in HIC experiments. In the equilibrium transition, the hadronic and quark phases are connected through the Gibbs conditions. This approach is widely used in the description of the phase transition in the neutron star with a quark core or kaon condensate [56–65]. It is also generalized to explore the phase transformation from nuclear to quark matter at finite density and temperature in HICs [66–76].

In our previous study [73–76], attention was focused on the isospin asymmetric matter, and some observable effects on isospin-relevant meson yield ratios were proposed. As a further study along this line, in this study we take a chemical potential dependent Polyakov loop potential in the PNJL model to construct the two-phase model and explore the full QCD phase diagram. Compared with the previous results in the original PNJL model, the calculation presents that the phase transition lines move towards low densities (small $\mu_B$). The transition region is possibly reached in the planed experiments at the facilities of NICA/FAIR/J-PARC and the BES II program at RHIC. We also analyze the transition signatures changing with the $\mu$-dependence of the Polyakov loop potential. This is another strong motivation to measure the mixed phase region in HIC experiments.

The paper is organized as follows. In Sec. II, we describe briefly the two-phase approach and give the relevant formulas of the hadron-$\mu$PNJL model. In Sec. III, we present the numerical results about the phase diagram of the equilibrated phase transition, and analyze the influence of the $\mu$-dependent Polyakov loop potential on the boundaries from nuclear to quark matter and transition signatures possibly observed in the next generation facilities. Finally, a summary is given in Sec. IV.

## II. THE MODELS

### A. Description of hadronic matter

The pure hadronic matter at low $T$ and small $\mu_B$ is described by the nonlinear Walecka-type model. The Lagrangian is given as

$$\mathcal{L}_H = \sum_N \bar{\psi}_N [i\gamma_\mu \partial^\mu - M + g_\sigma \sigma - g_\omega \gamma_\mu \omega^\mu - g_\rho \gamma_\mu \tau \cdot \boldsymbol{\rho}^\mu]\psi_N$$
$$+ \frac{1}{2}(\partial_\mu \sigma \partial^\mu \sigma - m_\sigma^2 \sigma^2) - V(\sigma) + \frac{1}{2}m_\omega^2 \omega_\mu \omega^\mu$$
$$- \frac{1}{4}\omega_{\mu\nu}\omega^{\mu\nu} + \frac{1}{2}m_\rho^2 \boldsymbol{\rho}_\mu \cdot \boldsymbol{\rho}^\mu - \frac{1}{4}\boldsymbol{\rho}_{\mu\nu} \cdot \boldsymbol{\rho}^{\mu\nu}, \quad (1)$$

where $\omega_{\mu\nu} = \partial_\mu \omega_\nu - \partial_\nu \omega_\mu$, $\boldsymbol{\rho}_{\mu\nu} \equiv \partial_\mu \boldsymbol{\rho}_\nu - \partial_\nu \boldsymbol{\rho}_\mu$. In this model, the interactions between nucleons are mediated by $\sigma$, $\omega$, $\boldsymbol{\rho}$ mesons. The self-interactions of the $\sigma$ meson, $V(\sigma) = \frac{1}{3}b(g_\sigma \sigma)^3 + \frac{1}{4}c(g_\sigma \sigma)^4$, are included to give the correct compression modulus, the effective nucleon mass at nuclear saturation density. The parameter set NL$\rho$ is used in the calculation, which gives a good description of the properties of nuclear matter. (The details can be found in Refs. [68–70,73,74,76].)

To describe asymmetric nuclear matter, we define the baryon and isospin chemical potential as

$$\mu_B^H = \frac{(\mu_p + \mu_n)}{2}, \qquad \mu_3^H = (\mu_p - \mu_n). \quad (2)$$

The asymmetry parameter of nuclear matter is defined as

$$\alpha^H = (\boldsymbol{\rho}_n - \boldsymbol{\rho}_p)/(\rho_p + \rho_n), \quad (3)$$

which is determined by the heavy ions taken in experiments. The values of $\alpha^H$ are compiled for some heavy-ion sources in [71], and the largest one is $\alpha^H = 0.227$ in the $^{238}\text{U} + ^{238}\text{U}$ collision for stable nuclei. For unstable nuclei, $\alpha^H$ can take a larger value.

### B. Description of quark matter

To describe pure quark matter at large $\mu_B$ and finite $T$, we use the recently developed chemical potential dependent PNJL model. First, we introduce the original PNJL model, and then consider the $\mu$-dependent Polyakov loop potential. The Lagrangian of the standard two-flavor PNJL model is

$$\mathcal{L}^Q = \bar{q}(i\gamma^\mu D_\mu - \hat{m}_0)q + G[(\bar{q}q)^2 + (\bar{q}i\gamma_5 \vec{\tau}q)^2]$$
$$- \mathcal{U}(\Phi[A], \bar{\Phi}[A], T), \quad (4)$$

where $q$ denotes the quark fields with two flavors, $u$ and $d$, and three colors; $\hat{m}_0 = \text{diag}(m_u, m_d)$ in flavor space. The covariant derivative in the Lagrangian is defined as $D_\mu = \partial_\mu - iA_\mu - i\mu_q \delta_\mu^0$. The gluon background field

$A_\mu = \delta_\mu^0 A_0$ is supposed to be homogeneous and static, with $A_0 = g\mathcal{A}_0^\alpha \frac{\lambda^\alpha}{2}$, where $\frac{\lambda^\alpha}{2}$ is $SU(3)$ color generators.

The effective potential $\mathcal{U}(\Phi[A], \bar{\Phi}[A], T)$ is expressed in terms of the traced Polyakov loop $\Phi = (\mathrm{Tr}_c L)/N_C$ and its conjugate $\bar{\Phi} = (\mathrm{Tr}_c L^\dagger)/N_C$. The Polyakov loop $L$ is a matrix in color space

$$L(\vec{x}) = \mathcal{P} \exp\left[i \int_0^{\frac{1}{T}} d\tau A_4(\vec{x}, \tau)\right], \tag{5}$$

where $A_4 = iA_0$.

The temperature-dependent Polyakov loop effective potential $\mathcal{U}(\Phi, \bar{\Phi}, T)$ proposed in [77] takes the form

$$\frac{\mathcal{U}(\Phi, \bar{\Phi}, T)}{T^4} = -\frac{a(T)}{2} \bar{\Phi}\Phi + b(T) \ln[1 - 6\bar{\Phi}\Phi + 4(\bar{\Phi}^3 + \Phi^3) - 3(\bar{\Phi}\Phi)^2], \tag{6}$$

where

$$a(T) = a_0 + a_1\left(\frac{T_0}{T}\right) + a_2\left(\frac{T_0}{T}\right)^2, \quad b(T) = b_3\left(\frac{T_0}{T}\right)^3. \tag{7}$$

The parameters $a_i$, $b_i$ summarized in Table I are precisely fitted according to the result of lattice QCD thermodynamics in pure gauge sector.

The parameter $T_0 = 270$ MeV is the confinement-deconfinement transition temperature in the pure Yang-Mills theory at vanishing chemical potential [78]. In the presence of fermions, the quantum backreaction of the matter sector to the glue sector should be considered, which leads to a flavor and quark chemical potential dependence of the transition temperature $T_0(N_f, \mu)$ ($\mu = \mu_u = \mu_d$ for symmetric quark matter) [51–55]. By using renormalization group theory in [51], the form of $T_0(N_f, \mu)$ is proposed with

$$T_0(N_f, \mu) = T_\tau e^{-1/(\alpha_0 b(N_f, \mu))}, \tag{8}$$

where

$$b(N_f, \mu) = \frac{11N_c - 2N_f}{6\pi} - \beta\frac{16N_f}{\pi}\frac{\mu^2}{T_\tau^2}. \tag{9}$$

The running coupling $\alpha_0 = 0.304$ is fixed at the $\tau$ scale $T_\tau = 1.770$ GeV according to the deconfinement transition

TABLE I.  Parameters in Polyakov effective potential given in [77].

| $a_0$ | $a_1$ | $a_2$ | $b_3$ |
|-------|-------|-------|-------|
| 3.51  | −2.47 | 15.2  | −1.75 |

temperature $T_0 = 270$ MeV of pure gauge field with $N_f = 0$ and $\mu = 0$. When fermion fields are included, $T_0$ is rescaled to 208 MeV for 2 flavor and 187 MeV for $2 + 1$ flavor at vanishing chemical potential. The parameter $\beta$ in Eq. (9) governs the curvature of $T_0(\mu)$ as a function of quark chemical potential.

With the consideration of the chemical potential dependence of Polyakov loop potential, this improved PNJL model is named the $\mu$PNJL model. We then replace the $T_0$ with $T_0(N_f, \mu)$ in the Polyakov loop potential given in Eq. (7). The thermodynamical potential of quark matter in the $\mu$PNJL model within the mean field approximation can be derived then as

$$\Omega = \mathcal{U}(\bar{\Phi}, \Phi, T) + G(\phi_u + \phi_d)^2 - 2\int_\Lambda \frac{d^3k}{(2\pi)^3} 3(E_u + E_d)$$
$$- 2T\sum_{u,d}\int \frac{d^3k}{(2\pi)^3}[\ln(1 + 3\Phi e^{-(E_i - \mu_i)/T} + 3\bar{\Phi}e^{-2(E_i - \mu_i)/T} + e^{-3(E_i - \mu_i)/T})]$$
$$- 2T\sum_{u,d}\int \frac{d^3k}{(2\pi)^3}[\ln(1 + 3\bar{\Phi}e^{-(E_i + \mu_i)/T} + 3\Phi e^{-2(E_i + \mu_i)/T} + e^{-3(E_i + \mu_i)/T})], \tag{10}$$

where $E_i = \sqrt{k^2 + M_i^2}$ is energy-momentum dispersion relation of quark flavor $i$, and $\mu_i$ is the corresponding quark chemical potential.

The dynamical quark masses and quark condensates are coupled with the following equations:

$$M_i = m_0 - 2G(\phi_u + \phi_d), \tag{11}$$

$$\phi_i = -2N_c \int \frac{d^3k}{(2\pi)^3}\frac{M_i}{E_i}(1 - n_i(k) - \bar{n}_i(k)), \tag{12}$$

where $n_i(k)$ and $\bar{n}_i(k)$

$$n_i(k) = \frac{\Phi e^{-(E_i - \mu_i)/T} + 2\bar{\Phi}e^{-2(E_i - \mu_i)/T} + e^{-3(E_i - \mu_i)/T}}{1 + 3\Phi e^{-(E_i - \mu_i)/T} + 3\bar{\Phi}e^{-2(E_i - \mu_i)/T} + e^{-3(E_i - \mu_i)/T}}, \tag{13}$$

$$\bar{n}_i(k) = \frac{\bar{\Phi} e^{-(E_i + \mu_i)/T} + 2\Phi e^{-2(E_i + \mu_i)/T} + e^{-3(E_i + \mu_i)/T}}{1 + 3\bar{\Phi}e^{-(E_i + \mu_i)/T} + 3\Phi e^{-2(E_i + \mu_i)/T} + e^{-3(E_i + \mu_i)/T}} \tag{14}$$

are modified Fermion distribution functions of quark and antiquark. The values of $\phi_u, \phi_d, \Phi$ and $\bar{\Phi}$ can be determined by minimizing the thermodynamical potential

$$\frac{\partial\Omega}{\partial\phi_u} = \frac{\partial\Omega}{\partial\phi_d} = \frac{\partial\Omega}{\partial\Phi} = \frac{\partial\Omega}{\partial\bar{\Phi}} = 0. \tag{15}$$

All the thermodynamic quantities relevant to the bulk properties of quark matter can be obtained from $\Omega$. Particularly, we note that the pressure and energy density should be zero in the vacuum. In the calculation a cutoff $\Lambda$ is implemented in 3-momentum space for divergent integrations. $\Lambda = 651$ MeV, $G = 5.04$ GeV$^{-2}$, $m_{u,d} = 5.5$ MeV will be taken by fitting the experimental values of pion decay constant $f_\pi = 92.3$ MeV and pion mass $m_\pi = 139.3$ MeV [33].

For asymmetric quark matter, the baryon and isospin chemical potential are defined as $\mu_B^Q = \frac{3}{2}(\mu_u + \mu_d)$, $\mu_3^Q = (\mu_u - \mu_d)$, respectively. The quark chemical potential $\mu$ in $T_0(N_f, \mu)$ can take the mean values of the $u$, $d$ quark. The asymmetry parameter of pure quark matter is

$$\alpha^Q = -\frac{\rho_3^Q}{\rho_B^Q} = -\frac{(\rho_u - \rho_d)}{(\rho_u + \rho_d)/3}, \qquad (16)$$

where $\rho_3^Q = (\rho_u - \rho_d)$, and $\rho_B^Q = (\rho_u + \rho_d)/3$.

### C. Transformation from hadronic to quark matter

The above is a separate description of the purely hadronic and quark matter. When the equilibrium transition between the hadronic and quark matter forms, the Gibbs' conditions with the thermal, chemical and mechanical equilibrium need to be satisfied (a general discussion of phase transitions in multicomponent systems can be found in Ref. [57]),

$$\mu_B^H = \mu_B^Q, \qquad \mu_3^H = \mu_3^Q, \qquad T^H = T^Q, \qquad P^H = P^Q, \qquad (17)$$

where $\mu_3^H$ and $\mu_3^Q$ are the isospin chemical potential of the hadronic and quark phase, separately. In the coexisting region, the total baryon density is consisted of two parts, $\rho_B = (1 - \chi)\rho_B^H + \chi\rho_B^Q$, where $\chi$ is the fraction of quark matter, and $1 - \chi$ is the ratio of nuclear matter. Similarly, $\rho_3 = (1 - \chi)\rho_3^H + \chi\rho_3^Q$ is the total isospin density.

As shown in the previous study [66–76], the phase transition features of asymmetric matter are isospin dependent. Once the species of heavy ions are chosen in HIC experiments, the asymmetry parameter will be determined. Due to the isospin conservation in strong interaction, the global asymmetry parameter $\alpha$,

$$\alpha \equiv -\frac{\rho_3}{\rho_B} = -\frac{(1 - \chi)\rho_3^H + \chi\rho_3^Q}{(1 - \chi)\rho_B^H + \chi\rho_B^Q}, \qquad (18)$$

for the mixed phase should maintain constant. However, in the coexisting region the local asymmetry parameters, $\alpha^H$ and $\alpha^Q$, can vary for a different quark fraction $\chi$. It is just the $\chi$-dependence of $\alpha^H$ and $\alpha^Q$ that provides the possibility to test the isospin relevant signals generated in the

hadronization stage in HIC experiments. The details about the phase transformation from asymmetric nuclear matter to quark matter will be discussed in the next section. One can also refer to our previous researches [69,73–76].

## III. NUMERICAL RESULTS AND DISCUSSIONS

### A. Features of pure quark matter in the $\mu$PNJL model

In this subsection, we present some properties of pure symmetric quark matter in the $\mu$PNJL model. First, we present in Fig. 1 the chemical potential dependence of $T_0(\mu)$. Different values of $\beta$ are used in the calculation for a tentative study. In the case of $\beta = 0$, corresponding to the standard PNJL model in which only the contribution from gauge field to Polyakov loop potential is considered, $T_0(\mu) = 208$ MeV is a constant, as shown with the solid line in Fig. 1. The dotted lines show the results for $\beta \neq 0$. This figure manifests that $T_0(\mu)$ is sensitive to $\beta$ which in some degree can be taken as a parameter to reflect the interaction strength between the matter sector and the glue sector.

Figure 2 presents the values of Polyakov loop $\Phi$ and $\bar{\Phi}$ as functions of baryon density for various $\beta$ at $T = 20$ MeV. In the original PNJL model (the case $\beta = 0$), $\Phi$ and $\bar{\Phi}$ always take small values at low temperature. This means that quarks are confined, even in the high density region where the chiral symmetry is restored already. This forms the so-called quarkyonic phase at low $T$ and high density region. However with the consideration of quark back-reaction to glue sector, quark confinement-deconfinement phase transition can occur at low $T$, as shown by the dotted lines with different values of $\beta$. If we take the standard that $\Phi$ or $\bar{\Phi} = 0.5$ marks the happening of deconfinement transition, as adopted in [32,39], we find the transition density moves to a lower one for a larger $\beta$. If we take $\beta \gg 1$ in the calculation, unphysical results will be derived with too small deconfined baryon density where the chiral symmetry is still breaking. For more details about the
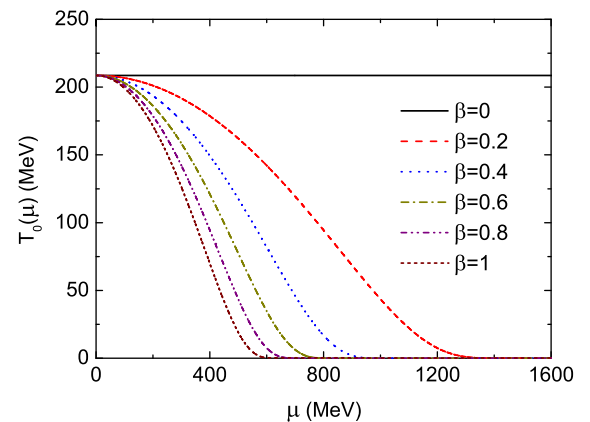


FIG. 1. $T_0(\mu)$ as a function of $\mu$ with various $\beta$ from 0 to 1. The case $\beta = 0$ corresponds to the standard PNJL model.
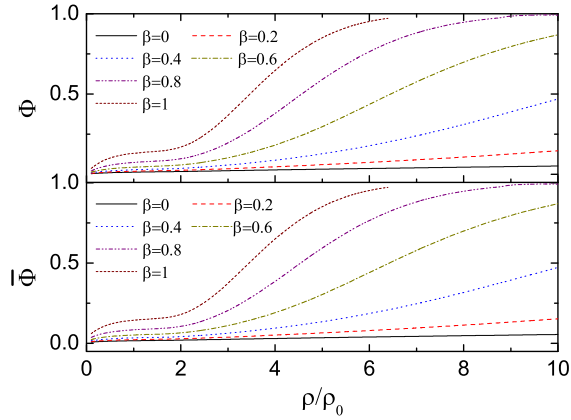
FIG. 2.   Polyakov loop $\Phi$ and $\bar{\Phi}$ as functions of baryon density $\rho_B$ for different $\beta$ at $T = 20$ MeV.



FIG. 3.   Phase diagram of the hadron-quark phase transition in the T-$\rho_B$ plane for different $\beta$ with the asymmetry parameter $\alpha = 0.2$.

properties of quark matter, one can refer to [54,55]. In this study we mainly emphasize the transformation from hadronic to quark matter at intermediate densities in the two-phase model.

### B. Transition boundaries from hadronic to quark matter in the two-phase model with different $\beta$

In this part we focus on the phase transition from asymmetric nuclear to quark matter in the two-phase model. Since the largest asymmetry parameter that can be reached for stable nuclei is $\alpha = 0.227$ in $^{238}$U + $^{238}$U collision, we choose $\alpha = 0.2$ and different $\beta$ to demonstrate the features of the phase transition of asymmetric matter. As a matter of fact, $\alpha$ can take a larger value for neutron-rich unstable nuclei.

The equilibrium phase transition is constructed based on Gibbs criteria given in Eq. (17) and the isospin charge conservation given in Eq. (18) for strong interaction. Figures 3 and 4 show the boundaries of hadron-quark transition in the $T - \rho_B$ and $T - \mu_B$ diagram with a series of $\beta$. For each value of $\beta$, the curves with the same color mark the boundaries of purely hadronic matter (at low densities) and purely quark matter (at high densities). For the equilibrium transition derived with the original PNJL model (the case $\beta = 0$), the transition lines as functions of $\rho_B$ and $\mu_B$ vary nonmonotonously with the increase of $T$. This feature maintains when a weak interaction between matter sector and glue sector is included, e.g., in the case of $\beta = 0.2$ and 0.4. But the transition lines as functions of $\rho_B$ and $\mu_B$ decrease monotonously when $\beta \geq 0.6$ is taken. These features indicate that the backreaction of the matter sector to the glue sector is crucial and indispensable for the hadron-quark phase transition.

In Figs. 3 and 4, the region between the curves with the same color for each $\beta$ is the hadron-quark coexisting phase. The transition in the coexisting phase is the first order because of the discontinuity of baryon density in the two phases. Figures 3 and 4 also present that, with the increase
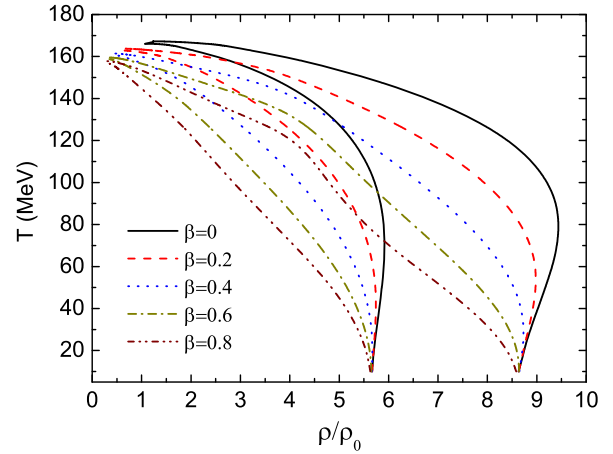
of $\beta$, the transition boundaries move towards smaller $\rho_B$ and $\mu_B$. In particular, the end point of the phase transition moves also towards lower $T$ with the increase of $\beta$. The main reason is that the confinement-deconfinement transition temperature $T_0(\mu)$ decreases to a lower value when a larger parameter of $\beta$ is taken, as shown in Fig. 1.

To further understand the effect of $\beta$ on the phase transition, we plot the $P - \mu_B$ phase diagram of symmetric nuclear and quark matter in Fig. 5. The solid and dashed curves are the pressure of pure hadronic and quark matter, respectively. The solid dots indicate the locations of the hadron-quark phase transition where the Gibbs criteria are fulfilled at different conditions. For a given temperature, we can see that the phase transition (solid dot) moves to a smaller $\mu_B$ with the increase of $\beta$. The reason is the pressure of quark matter increases more quickly when a larger $\beta$ is taken, and then the mechanical equilibrium can be reached
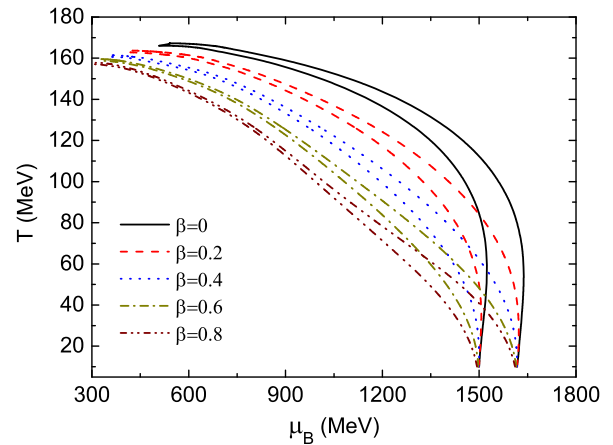


FIG. 4.   Phase diagram of the hadron-quark phase transition in the T-$\mu_B$ plane for different $\beta$ with the asymmetry parameter $\alpha = 0.2$.
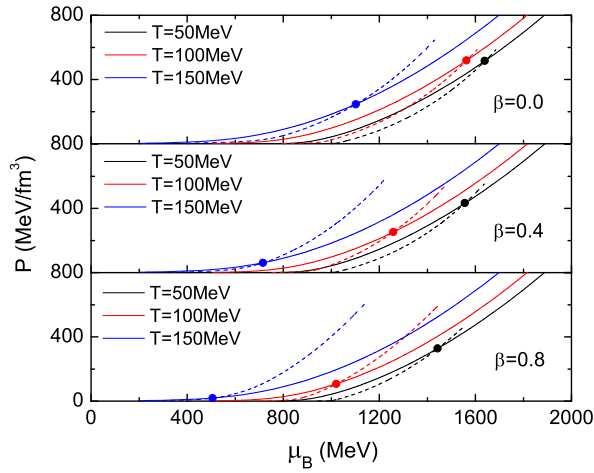
FIG. 5. Pressure of symmetric hadronic (solid) and quark pressure (dashed) as functions of baryon chemical potential at $T = 50$, 100 and 150 MeV for several $\beta$.

at a smaller $\mu_B$. On the other hand, for a given $\beta$, with the increase of temperature the phase transition also moves towards a smaller $\mu_B$, since the increase of the pressure of quark matter is faster than that of hadronic matter. The intersection point (solid dot) will finally vanish when the temperature is higher than a critical value beyond which the pressure of quark phase will be always higher than that of the hadronic phase, then the phase equilibrium cannot be reached any more. Therefore, there is an end point and the mixed phase finally disappears at high temperature in the two-phase model.

Similar results can be obtained for asymmetric matter. In addition, we note that there is a critical value of $\beta = 0.89$. For the case $\beta > 0.89$, the equilibrium transition cannot be realized for $\alpha = 0.2$ in the two-phase model. The measurement of the mixed phase in HIC experiments possibly provides relevant information on the $\beta$ parameter, i.e. on the $\mu$-dependence of the Polyakov loop potential.

Furthermore, we give a comparison of the phase transition in the $\mu$PNJL model and the two-phase model. The confinement-deconfinement phase transition can be realized at low $T$ in the $\mu$PNJL model, but the threshold depends on the parameter $\beta$, which reflects the interaction strength of the matter sector to the glue sector. Compared with the two-phase model, if a smaller $\beta$ is taken, the onset density of deconfinement phase transition in the $\mu$PNJL model will be larger than that in the two-phase model. But the phase transition line moves towards lower densities with the increase of $\beta$. The onset density can be even smaller than that of the two-phase model if $\beta$ is large enough.

For the case $\beta = 0.4$ or smaller, when the hadron-quark phase transition happens in the two-phase model as shown in Fig. 3, the values of $\Phi$ and $\bar{\Phi}$ in the quark phase are still smaller than 0.5 as shown in Fig. 2, it seems that the two-phase model predicts a transition to confined quark matter.

The appearance of such a behavior is attributed to the quark model. We know that in the original PNJL model the confinement-deconfinement phase transition cannot be realized at very low $T$ because $\Phi$ and $\bar{\Phi}$ always take small values. This is one of the most important reasons that motivate us to take the $\mu$PNJL model. However, even in the $\mu$PNJL model with $\beta = 0.4$ or smaller, the confinement-deconfinement phase transition at low $T$ can only happen at very high baryon number densities. This explains why it seems that the two-phase model predicts a transition to confined quark matter for a small $\beta$ in the two-phase model. In principle, the two-phase model describes the phase equilibrium where quarks have deconfined. From this point of view, in the two-phase model the results derived with $\beta = 0.4$ or smaller are unphysical. Therefore, it is necessary to introduce the $\mu$-dependent $T_0$ and take a value of $\beta$ larger than 0.4, which also means the backreaction of matter to glue sector is strong at finite densities.

We also note that the two kinds of phase transitions are constructed in different methods. The two-phase model describes the equilibrium phase transition possibly reached during the formation of quark matter in heavy-ion collisions. The deconfinement phase transition in the PNJL or $\mu$PNJL quark model is derived based on the quark-gluon degrees of freedom. To what degree the phase transition from deconfinement to confinement in the quark model can be identified with the formation of hadronic matter is still not clear. For example, there exists the so-called quarkyonic phase in the PNJL model where the chiral symmetry has restored but quarks are still confined at low $T$, and the "coincidence problem" exists at high $T$. We emphasize that related discussions are still open issues. The experiments in the future will provide us more information about the phase transition.

### C. Effects of isospin asymmetry

Now we discuss the influence of asymmetry parameter $\alpha$ on the phase diagram. Different values of $\alpha$ correspond to different kinds of heavy-ion sources chosen in HIC experiments. Considering the unstable nuclei, $\alpha$ can take a value larger than 0.227. Therefore, we take the values of $\alpha$ between 0 and 0.35 in the calculation to show the isospin effect.

We plot the phase diagram of equilibrium transition from asymmetric hadronic to quark matter in Figs. 6 and 7 in the two-phase model. In the two figures, the upper panels are the results of the original PNJL model. The lower panels are the results of the $\mu$-dependent PNJL model with the contribution of both matter sector and glue sector with $\beta = 0.8$. In addition to the conclusion derived in the last subsection, the two figures show that the onset densities (chemical potentials) move to smaller ones with the increase of asymmetry parameter $\alpha$, and the corresponding coexisting region enlarges. On the other hand, for each value of $\alpha$ the coexisting region shrinks greatly at high
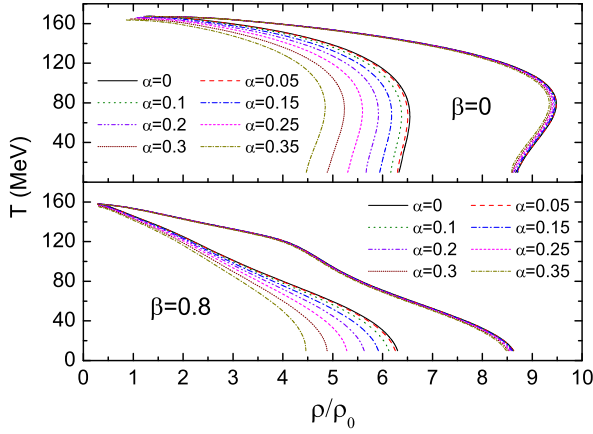
FIG. 6. Phase diagrams of the hadron-quark phase transition in the T-$\rho_B$ plane with various asymmetry parameters for $\beta = 0$ (upper panel) and $\beta = 0.8$ (lower panel).
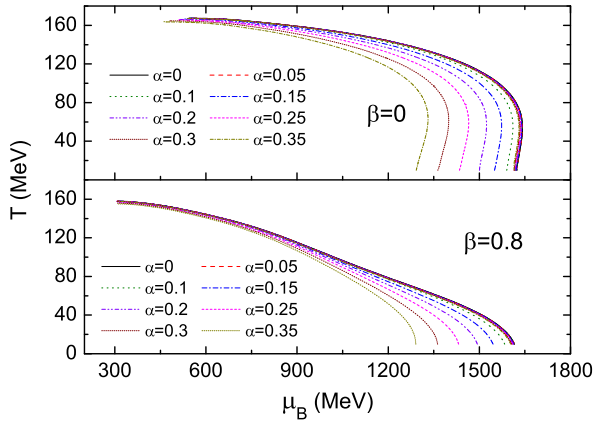


FIG. 8. Critical behavior of the hadron-quark phase transition for symmetric and asymmetric matter with different $\alpha, \beta$.



FIG. 7. Phase diagrams of the hadron-quark phase transition in the T-$\mu_B$ plane with various asymmetry parameters for $\beta = 0$ (upper panel) and $\beta = 0.8$ (lower panel).

temperature. We note that for symmetric matter (the case $\alpha = 0$), only one transition line but not transition region exists in the $T - \mu_B$ diagram.

To show more clearly how the asymmetry parameter $\alpha$ affects the phase transition near the end point, we present in Fig. 8 the details of the $T - \rho_B$ phase diagram in the high-temperature region. The upper panels of Fig. 8 are the results of symmetric matter with $\alpha = 0$, and the middle and lower panels are the results of asymmetric matter with $\alpha = 0.2$ and 0.3, respectively. The upper panels shows that the boundaries of $\chi = 0$ and $\chi = 1$ have the same end point at high temperature for symmetric matter. However, for asymmetric matter, the locations of the end points for $\chi = 0$ and $\chi = 1$ are slightly different for asymmetric matter, as shown with the solid dots in the middle panels for $\alpha = 0.2$ and in the lower panels for $\alpha = 0.3$. In Figs. 6 and 7 (including also the relevant phase diagram in our previous study [73–76]) only the boundaries with $\chi = 0$ and $\chi = 1$
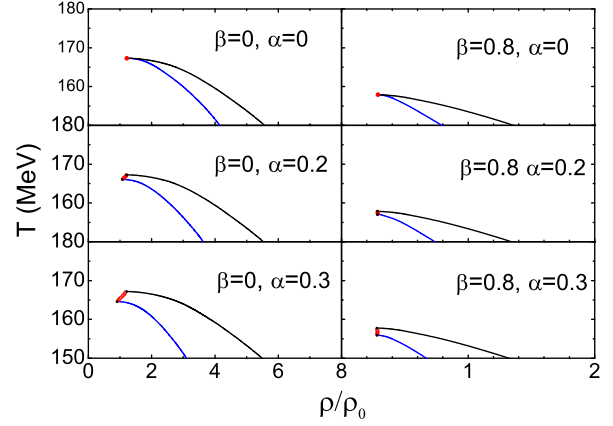
are plotted. As a matter of fact, we can find an end point for each value of $\chi$ in the region $0 < \chi < 1$. For a given $\chi$ in the calculation, before the end point is reached, $\rho_B^H < \rho_B^Q$ can be derived for the phase equilibrium in the mixed phase. The two curves of $T - \rho_B^H$ and $T - \rho_B^Q$ intersect at one point (the end point) at high T. Therefore, there exists a critical end point for each $\chi$ for asymmetric matter. It means that the end point is $\chi$ dependent for asymmetric matter. If these end points for different $\chi$ are connected, a short phase transition line forms as shown with the red bubbles in the middle and lower panels in Fig. 8.

## D. Isospin distillation effect in the mixed phase and observables in the hadronization

Now we discuss the isospin distillation effect in the hadron-quark coexisting phase of asymmetric matter. It is related to the isospin-relevant observables in the hadronization process. In the two-phase model, the asymmetry parameter $\alpha$ is globally conserved in the mixed phase, but the local asymmetry parameter $\alpha^H$ and $\alpha^Q$ can vary with the changing of quark fraction $\chi$ during the phase transition. We fix $\alpha = 0.2$ in the following calculation to explore the isospin distillation effect with different $\beta$. We note that the results for $\beta > 0.4$ are required with the presupposition that the phase transition is from nuclear matter to deconfined quark matter.

Figure 9 shows the local asymmetry parameter $\alpha^Q$ as a function of $T$ at the beginning of the transition with $\chi = 0.01$ for different values of $\beta$. This figure demonstrates that $\alpha^Q$ decreases with the increase of $\beta$. This behavior is relevant to the symmetry energy of both nuclear and quark matter. Our previous calculation [73] shows that the symmetry energy of nuclear matter increases quickly with the rising baryon density, but that of quark matter increases slightly. When a larger $\beta$ is taken to construct the equilibrium transition, the phase equilibrium moves to smaller $\rho_B$ and $\mu_B$ as shown in Figs. 3 and 4. Then the
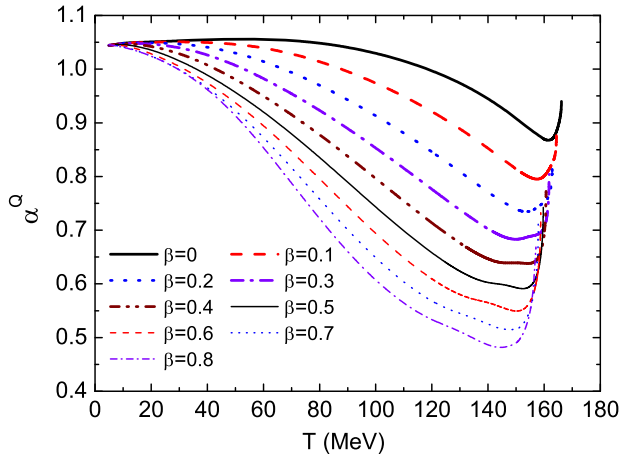
FIG. 9. Local isospin asymmetry parameter $\alpha^Q$ in the mixed phase with quark fraction $\chi = 0.01$ as a function of temperature for various $\beta$ with the global asymmetry parameter $\alpha = 0.2$.

difference of the symmetry energy between nuclear and quark matter at low density (small $\mu_B$) is relatively smaller, which results in the reduction of $\alpha^Q$. For more details, one can refer to [73].

Figure 9 also presents that for each $\beta$ there is an inflection point of $\alpha^Q$ in the region of high $T$ (corresponding to low $\rho_B$ and small $\mu_B$). This behavior reflects the relations between dynamical quark mass and $u$, $d$ quark chemical potential. To see more clearly this phenomenon, we plot in Fig. 10 the evolution curves of the dynamical quark mass and $u$, $d$ quark chemical potential (upper panel) as well as the ratio of $\rho_d/\rho_u$ (lower panel), as functions of temperature in the mixed phase with a fixed $\chi = 0.01$. Figure 10 shows that the dynamical quark mass in the equilibrium transition increases with the rising $T$ (towards low $\rho_B$ and small $\mu_B$). It implies that the chiral dynamics is affected by both temperature and density (chemical
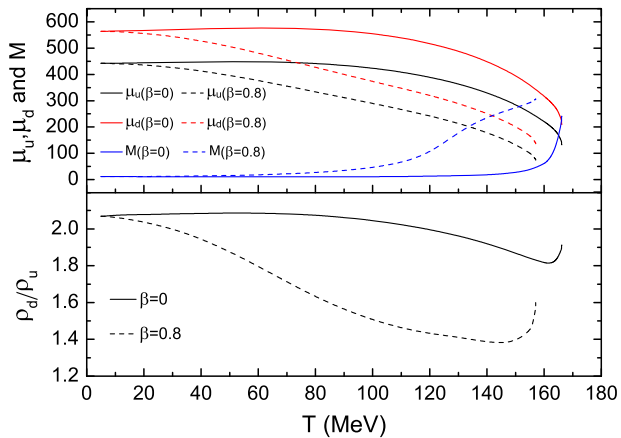


FIG. 10. (upper panel) $u$, $d$ quark chemical potentials and dynamical quark mass as well as $\rho_d/\rho_u$ (lower panel) as functions of $T$ inside the mixed phase at $\chi = 0.01$ with $\alpha = 0.2$ for $\beta = 0$ and $\beta = 0.8$, respectively.

potential). From Fig. 10 we can also see that both $u$ and $d$ quark chemical potentials decrease with the rising $T$. Because $\mu_u$ is smaller than $\mu_d$, the intersection of the curves of $\mu_u$ and quark mass $M$ appear at a relatively lower $T$ than that of $\mu_d$ and $M$. If the system is a simple fermion system with the fermion distribution function $f = 1/(1 + e^{(E-\mu)/T})$, $\rho_u$ will sharply decrease when $\mu_u$ is smaller than the dynamical quark mass $M$ at low $T$. Correspondingly, an inflection point of $\alpha^Q$ [with the definition of $\alpha^Q = (\rho_d - \rho_u)/(\rho_u + \rho_d)/3$] at the intersection point of $\mu_u$ and $M$ should appear. However, such a behavior is not seen in Fig. 10. As a matter of fact, for $\beta = 0.8$ (0), the fast increase of $\rho_d/\rho_u$ occurs for temperatures larger (smaller) than the one corresponding to the crossing point of $\mu_u$ and $M$. The deviation of the inflection point from $\mu_u = M$ shows that the quark system cannot be taken as a simple fermion system. There exists complex interactions as indicated by the quark distribution function given in Eq. (13). Besides $\mu$ and $M$, Eq. (13) indicates that the quark distribution function is also relevant to $\Phi$ and $\bar{\Phi}$ which are affected by the temperature and quark chemical potential (i.e., by the parameter $\beta$). On the other hand, since the temperature at the inflection point is in the region about (150–165) MeV, the thermal excitation to some degree alleviates the fast decrease of the quark distribution function at the crossing point of $\mu_u = M$. Therefore, the location of the inflection point is much more complex than that in a simple fermion system.

If the phase equilibrium can be reached in HIC experiments, the generated quarks will recombine into hadrons in the later hadronization process, and a sudden increase of isospin relevant meson yield ratio such as $\pi^-/\pi^+$, $K^0/K^+$ possibly be observed since the isospin enrichment in the quark phase is well present (in particular in the initial part of the mixed phase). The strength of these signals depends on the value of $\alpha^Q$ (or $\rho_d/\rho_u$) which is relevant to the parameter $\beta$ in the $\mu$PNJL model. Compared with the original PNJL model, the introduction of $\mu$-dependent Polyakov loop potential (with $\beta > 0.4$) will weaken the isospin relevant signals at high $T$, leading to a relatively smaller ratio of $\pi^-/\pi^+$, $K^0/K^+$. However, the isospin effect is still distinct at low $T$ as demonstrated in Fig. 9 and the lower panel of Fig. 10. There is also an inflection point of these isospin relevant signals at high temperature as indicated in Figs. 9 and 10. For more discussion about the phase transition signatures in the two-phase model, one can refer to [79] prepared for the NICA white paper.

Due to the isospin conservation during the phase transition with strong interaction, the global isospin asymmetry parameter $\alpha$ given by Eq. (18) for the mixed phase includes the contribution from both nuclear and quark component. For a given heavy ion source in HIC experiments, i.e., a given $\alpha$, if the local asymmetry parameter $\alpha^Q$ is larger when the equilibrium is reached, the local asymmetry parameter $\alpha^H$ will be reduced, and vice versa.

The value of $\alpha^Q$ reached in the coexisting phase determines the production of isospin-rich meson resonances and subsequent decays in the hadronization process. Simultaneously, the value of $\alpha^H$ of the nuclear component determines the emission of neutron-rich clusters in the collision. Therefore, the ratio of isospin relevant meson (e.g., $\pi^-/\pi^+$) and neutron-rich cluster production have an opposite tendency when the mixed phase forms in experiments. In the hadron-PNJL model, the emission of neutron-rich cluster is reduced because of the larger isospin trapping (larger $\alpha^Q$) in the quark component of the mixed phase. But in the hadron-$\mu$PNJL model with $\beta > 0.4$, the isospin asymmetry of $u$, $d$ quark decreases greatly at high temperature. Correspondingly, the neutron-rich clusters will increase in comparison with the case of the hadron-PNJL model. In fact, in the two-phase model, only the results given by $\beta > 0.4$ fulfill the requirement that the phase transition is from nuclear matter to deconfined quark matter as discussed in Sec. III B. Therefore, a combination of the isospin relevant observables including both isospin mesons and neutron-rich clusters in HIC experiments can be used to constrain the value of $\beta$. What is more, a detailed analysis of the generated particles in the transport theory for heavy ion collision is deserving for further study.

From Fig. 9 we can also see that the value of $\alpha^Q$ is $T$ dependent, which means the strength of isospin relevant signatures depends on the beam energy in experiments. To look for the location of the critical end point and the critical behaviors, the second stage of the beam energy scan (BES II) will be performed on RHIC soon. Relevant experiments at intermediate densities is also in the plan on NICA/FAIR/J-PACK. In particular, J-PACK experiments will focus on the low-$T$ and high-density region. Therefore, the beam energy scan will be performed in a wide energy range and the relevant signals can be measured in the next generation facilities. Through mapping the isospin effects of generated hadrons it provides an optional method to explore the transition boundaries from nuclear to quark matter.

We also note that the vector interactions between quarks are not included in this study. We have discussed elaborately the role of vector interactions on the phase transition in our previous research [75]. The calculation shows that with the inclusion of isoscalar-vector interaction the transition will move towards higher densities (chemical potential). Then the asymmetry parameter $\alpha^Q$

in the mixed phase will be enhanced due to the enlargement of the imbalance of symmetry energy in the two phases. For more details, one can refer to [73,76].

## IV. SUMMARY

We have studied the properties of quark matter in the improved PNJL model with the chemical potential dependent Polyakov loop potential which reflects to some degree the backreaction of the matter sector to the glue sector. Compared with the original PNJL model, a superiority of the $\mu$PNJL model is that it can effectively describe the confinement-deconfinement transition at low $T$ and high density region.

Furthermore, we constructed the hadron-$\mu$PNJL two-phase model, and use it to explore the equilibrium transition from asymmetric nuclear matter to quark matter. We derived the boundaries of the phase transition and analyzed the isospin-relevant signatures deduced from the two-phase model. Compared with the hadron-PNJL model, the calculation shows that the transition curves move to lower density (smaller chemical potential) when the $\mu$-dependent Polyakov loop potential is taken. Correspondingly, the isospin asymmetry in the quark component decreases at high $T$ for a larger $\beta$, which leads to a reduced ratio of $\pi^-/\pi^+$, $K^0/K^+$, but these observables are not sensitive to $\beta$ at low $T$. In the future, good data on the location of the mixed phase observed in HIC experiments will give valuable information on the $\mu$-dependence of the Polyakov loop potential. In particular, we suggest to measure the isospin-relevant signatures in the next generation accelerators such as NICA, FAIR and J-PACK, as well as the BES II program on RHIC, which would be helpful to explore the strongly interacting matter. In addition, the research deserves to be extended to investigate the evolution of the protoneutron star, which will be done as a further study.

## ACKNOWLEDGMENTS

[1] S. Gupta, X. F. Luo, B. Mohanty, H. G. Ritter, and N. Xu, Science **332**, 1525 (2011).

[2] P. Braun-Munzinger and J. Wambach, Rev. Mod. Phys. **81**, 1031 (2009).

[3] K. Fukushima and T. Hatsuda, Rep. Prog. Phys. **74**, 014001 (2011).

[4] F. Karsch, E. Laermann, and A. Peikert, Nucl. Phys. **B605**, 579 (2001).

[5] F. Karsch, Nucl. Phys. **A698**, 199 (2002).

[6] O. Kaczmarek and F. Zantow, Phys. Rev. D **71**, 114510 (2005).

[7] C. R. Allton, S. Ejiri, S. J. Hands, O. Kaczmarek, F. Karsch, E. Laermann, C. Schmidt, and L. Scorzato, Phys. Rev. D **66**, 074507 (2002).

[8] M. Cheng, N. H. Christ, S. Datta *et al.*, Phys. Rev. D **74**, 054507 (2006).

[9] Y. Aoki, S. Borsányi, S. Dürr, Z. Fodor, S. D. Katz, S. Krieg, and K. Szabo, J. High Energy Phys. 06 (2009) 088.

[10] Z. Fodor, S. D. Katz, and C. Schmidt, J. High Energy Phys. 03 (2007) 121.

[11] M. D'Elia and F. Sanfilippo, Phys. Rev. D **80**, 014502 (2009).

[12] S. Ejiri, Phys. Rev. D **78**, 074507 (2008).

[13] M. A. Clark and A. D. Kennedy, Phys. Rev. Lett. **98**, 051601 (2007).

[14] C. D. Roberts and S. M. Schmidt, Prog. Part. Nucl. Phys. **45**, S1 (2000).

[15] R. Alkofer and L. von Smekal, Phys. Rep. **353**, 281 (2001).

[16] C. S. Fischer, J. Phys. G **32**, R253 (2006).

[17] P. Maris and C. D. Roberts, Int. J. Mod. Phys. E **12**, 297 (2003).

[18] I. C. Clöt and C. D. Roberts, Prog. Part. Nucl. Phys. **77**, 1 (2014).

[19] S. S. Xu, Z. F Cui, B. Wang, Y. M. Shi, Y. C. Yang, and H. S. Zong, Phys. Rev. D **91**, 056003 (2015).

[20] T. Hatsuda and T. Kunihiro, Phys. Lett. **145B**, 7 (1984).

[21] S. P. Klevansky, Rev. Mod. Phys. **64**, 649 (1992).

[22] T. Hatsuda and T. Kunihiro, Phys. Rep. **247**, 221 (1994).

[23] R. Alkofer, H. Reinhardt, and H. Weigel, Phys. Rep. **265**, 139 (1996).

[24] M. Buballa, Phys. Rep. **407**, 205 (2005).

[25] P. Rehberg, S. P. Klevansky, and J. Hüfner, Phys. Rev. C **53**, 410 (1996).

[26] M. Huang and I. Shovkovy, Nucl. Phys. **A729**, 835 (2003).

[27] M. Alford, A. Schmit, K. Rajagopal, and T. Schäfer, Rev. Mod. Phys. **80**, 1455 (2008).

[28] P. C. Chu, X. Wang, L. W. Chen, and M. Huang, Phys. Rev. D **91**, 023003 (2015).

[29] G. Q. Cao, L. Y. He, and P. F. Zhuang, Phys. Rev. D **90**, 056005 (2014).

[30] D. P. Menezes, M. B. Pinto, L. B. Castro, P. Costa, and C. Providência, Phys. Rev. C **89**, 055207 (2014).

[31] J. Xu, T. Song, C. M. Ko, and F. Li, Phys. Rev. Lett. **112**, 012301 (2014).

[32] K. Fukushima, Phys. Lett. B **591**, 277 (2004); Phys. Rev. D **77**, 114028 (2008).

[33] C. Ratti, M. A. Thaler, and W. Weise, Phys. Rev. D **73**, 014019 (2006).

[34] P. Costa, M. C. Ruivo, C. A. de Sousa, and H. Hansen, Symmetry **2**, 1338 (2010).

[35] K. Kashiwa, H. Kouno, M. Matsuzaki, and M. Yahiro, Phys. Lett. B **662**, 26 (2008).

[36] W. J. Fu, Z. Zhang, and Y. X. Liu, Phys. Rev. D **77**, 014006 (2008).

[37] S. K. Ghosh, S. Raha, R. Ray, K. Saha, and S. Upadhaya, Phys. Rev. D **91**, 054005 (2015).

[38] M. Dutra, O. Lourenço, A. Delfino, T. Frederico, and M. Malheiro, Phys. Rev. D **88**, 114013 (2013).

[39] Y. Sakai, T. Sasaki, H. Kouno, and M. Yahiro, Phys. Rev. D **82**, 076003 (2010).

[40] Y. Sakai, T. Sasaki, H. Kouno, and M. Yahiro, J. Phys. G **39**, 035004 (2012).

[41] T. Sasaki, J. Takahashi, Y. Sakai, H. Kouno, and M. Yahiro, Phys. Rev. D **85**, 056009 (2012).

[42] T. E. Restrepo, J. C. Macias, M. B. Pinto, and G. N. Ferrari, Phys. Rev. D **91**, 065017 (2015).

[43] T. Sasaki, Y. Sakai, H. Kouno, and M. Yahiro, Phys. Rev. D **84**, 091901(R) (2011).

[44] R. Gatto and M. Ruggieri, Phys. Rev. D **83**, 034016 (2011).

[45] M. Ferreira, P. Costa, and C. Providência, Phys. Rev. D **89**, 036006 (2014).

[46] B.-J. Schaefer, M. Wagner, and J. Wambach, Phys. Rev. D **81**, 074013 (2010).

[47] V. Skokov, B. Friman, and K. Redlich, Phys. Rev. C **83**, 054904 (2011).

[48] S. Chatterjee and K. A. Mohan, Phys. Rev. D **85**, 074018 (2012).

[49] L. McLarren and R. D. Pisarski, Nucl. Phys. **A796**, 83 (2007).

[50] Y. Hidaka, L. McLarren, and R. D. Pisarski, Nucl. Phys. **A808**, 117 (2008).

[51] B.-J. Schaefer, J. M. Pawlowski, and J. Wambach, Phys. Rev. D **76**, 074023 (2007).

[52] T. K. Herbst, J. M. Pawlowski, and B.-J. Schaefer, Phys. Lett. B **696**, 58 (2011).

[53] T. K. Herbst, J. M. Pawlowski, and B.-J. Schaefer, Phys. Rev. D **88**, 014007 (2013).

[54] H. Abuki, R. Anglani, R. Gatto, G. Nardulli, and M. Ruggieri, Phys. Rev. D **78**, 034034 (2008).

[55] X. Y. Xin, S. X. Qin, and Y. X. Liu, Phys. Rev. D **89**, 094012 (2014).

[56] N. K. Glendenning and S. A. Moszkowski, Phys. Rev. Lett. **67**, 2414 (1991); N. K. Glendenning, *Compact Stars* (Springer-Verlag, Berlin, 2000).

[57] N. K. Glendenning, Phys. Rev. D **46**, 1274 (1992).

[58] N. K. Glendenning and J. Schaffner-Bielich, Phys. Rev. Lett. **81**, 4564 (1998); Phys. Rev. C **60**, 025803 (1999).

[59] G. F. Burgio, M. Baldo, P. K. Sahu, and H.-J. Schulze, Phys. Rev. C **66**, 025802 (2002).

[60] T. Maruyama, S. Chiba, H.-J. Schulze, and T. Tatsumi, Phys. Rev. D **76**, 123015 (2007).

[61] F. Yang and H. Shen, Phys. Rev. C **77**, 025801 (2008).

[62] G. Y. Shao and Y. X. Liu, Phys. Rev. C **82**, 055801 (2010); G. Y. Shao, Phys. Lett. B **704**, 343 (2011).

[63] J. Xu, L. W. Chen, C. M. Ko, and B. A. Li, Phys. Rev. C **81**, 055803 (2010).

[64] V. A. Dexheimer and S. Schramm, Phys. Rev. C **81**, 045201 (2010).

[65] G. Y. Shao, M. Colonna, M. Di Toro, Y. X. Liu, and B. Liu, Phys. Rev. D **87**, 096012 (2013).

[66] H. Müller, Nucl. Phys. **A618**, 349 (1997).

[67] M. Di Toro, A. Drago, T. Gaitanos, V. Greco, and A. Lavagno, Nucl. Phys. **A775**, 102 (2006).

[68] M. Di Toro *et al.*, Prog. Part. Nucl. Phys. **62**, 389 (2009).

[69] M. Di Toro, B. Liu, V. Greco, V. Baran, M. Colonna, and S. Plumari, Phys. Rev. C **83**, 014911 (2011).

[70] B. Liu, M. Di Toro, G. Y. Shao, V. Greco, C. W. Shen, and Z. H. Li, Eur. Phys. J. A **47**, 104 (2011).

[71] R. Cavagnoli, C. Providência, and D. P. Menezes, Phys. Rev. C **83**, 045201 (2011).

[72] G. Pagliara and J. Schaffner-Bielich, Phys. Rev. D **81**, 094024 (2010).

[73] G. Y. Shao, M. Di Toro, B. Liu, M. Colonna, V. Greco, Y. X. Liu, and S. Plumari, Phys. Rev. D **83**, 094033 (2011).

[74] G. Y. Shao, M. Di Toro, V. Greco, M. Colonna, S. Plumari, B. Liu, and Y. X. Liu, Phys. Rev. D **84**, 034028 (2011).

[75] G. Y. Shao, M. Colonna, M. Di Toro, B. Liu, and F. Matera, Phys. Rev. D **85**, 114017 (2012).

[76] G. Y. Shao, Z. D. Tang, M. Di Toro, M. Colonna, X. Y. Gao, N. Gao, and Y. L. Zhao, Phys. Rev. D **92**, 114027 (2015).

[77] S. Rößner, C. Ratti, and W. Weise, Phys. Rev. D **75**, 034007 (2007).

[78] M. Fukugita, M. Okawa, and A. Ukava, Nucl. Phys. **B337**, 181 (1990).

[79] M. Di Toro, M. Colonna, V. Greco, and G. Y. Shao, arXiv:1601.05714.